Orientation of the crescent image of M87*

Krzysztof Nalewajko[1] and Agata Różańska[1]

1. Nicolaus Copernicus Astronomical Center, Bartycka 18, 00-716 Warszawa, Poland; knalew@camk.edu.pl

The first image of the black hole (BH) M87* obtained by the Event Horizon Telescope (EHT; EHT Collaboration et al. 2019a) has the shape of a crescent extending from the E to SWW position angles, while the observed direction of the large-scale jet is NWW (Walker et al., 2018). Comparing the EHT observed image with images based on numerical simulations of BH accretion flows suggests that on average the projected BH spin axis should be oriented SSW (EHT Collaboration et al., 2019b). Alternatively, if the spin axis is matched with the jet direction, emission from the SEE sector of the photon ring can only be accounted for as a temporary fluctuation. We explore highly simplified toy models for geometric distribution and kinematics of emitting regions in the Kerr metric, and perform ray tracing to calculate images. We strictly assume that: (1) the BH spin vector is fixed to the jet axis (position angle $\mathrm{PA_{jet}} = 288^\circ$, inclination $i = 162^\circ$), (2) the emitting regions are stationary and symmetric with respect to the BH spin, (3) the emissivities are isotropic in the local rest frames. Emission from the crescent sector SSE - SWW can be readily explained in terms of an equatorial ring with either circular or plunging geodesic flows, regardless of the value of BH spin. In the case of plane-symmetric polar caps with plunging geodesic flows, the dominant image of the cap located behind the BH is sensitive to the angular momentum of the emitter. Within the constraints of our model, we have not found a viable explanation for the observed brightness of the SEE sector. We conclude that the SEE emission should indeed be interpreted as a temporary departure from intrinsic axial symmetry of the inner accretion flow.

Methods. We perform ray tracing of BH image in the Kerr metric for BH mass M and spin a using the Boyer-Lindquist coordinates $x^\mu = (t, r, \theta, \phi)$. The emitting regions are assumed to be optically thin with uniform isotropic emissivities with power-law spectrum $j_{\rm em}(\nu_{\rm em}) \propto \nu_{\rm em}^{-\alpha}$ with spectral index $\alpha = 0.5$ in their local rest frames. The emission mechanism is not specified, and no absorption of radiation is considered. The emitters are allowed to be in motion relative to the local stationary observer with radial velocity $\beta_r = {\rm d}r/{\rm d}t$ and angular velocity $\Omega = {\rm d}\phi/{\rm d}t$, hence their 4-velocity is $u^\mu_{\rm em} = u^t_{\rm em}(1, \beta_r, 0, \Omega)$. From the covariant radiative transfer equation ${\rm d}_\lambda(I_\nu/\nu^3) = j_\nu/\nu^2$, for every geodesic $\mathcal{G}$ that intersects the emitting region $\mathcal{S}$, the observed intensity is integrated as being proportional to $I_{\nu,\rm obs} \propto \int_{\mathcal{G}\cap\mathcal{S}} {\rm d}\lambda\, g^{2+\alpha}$, where $g = [p_\mu(\lambda_{\rm obs})u^\mu_{\rm obs}]/[p_\mu(\lambda_{\rm em})u^\mu_{\rm em}]$ is the factor that combines gravitational redshift with the Doppler boost due to the motion of the emitter. The obtained images are scaled in the units of $\theta_{\rm g} = \arcsin(M/r_{\rm obs})$, Gaussian-smoothed with the angular resolution of $5.3\theta_{\rm g} \simeq 20$ μas, and normalised to the peak of the flux density of the EHT image.

We consider stationary emitting regions that are axisymmetric with respect to the BH spin axis and plane-symmetric with respect to the BH equatorial plane. In particular, we consider regions defined by $r \le r_{\rm max}$ and $0 \le \theta_{\rm min} \le \theta \le \theta_{\rm max} \le \pi/2$ (as well as $\theta_{\rm min} \le (\pi - \theta) \le \theta_{\rm max}$ for planar symmetry). In our calculations, we adopt

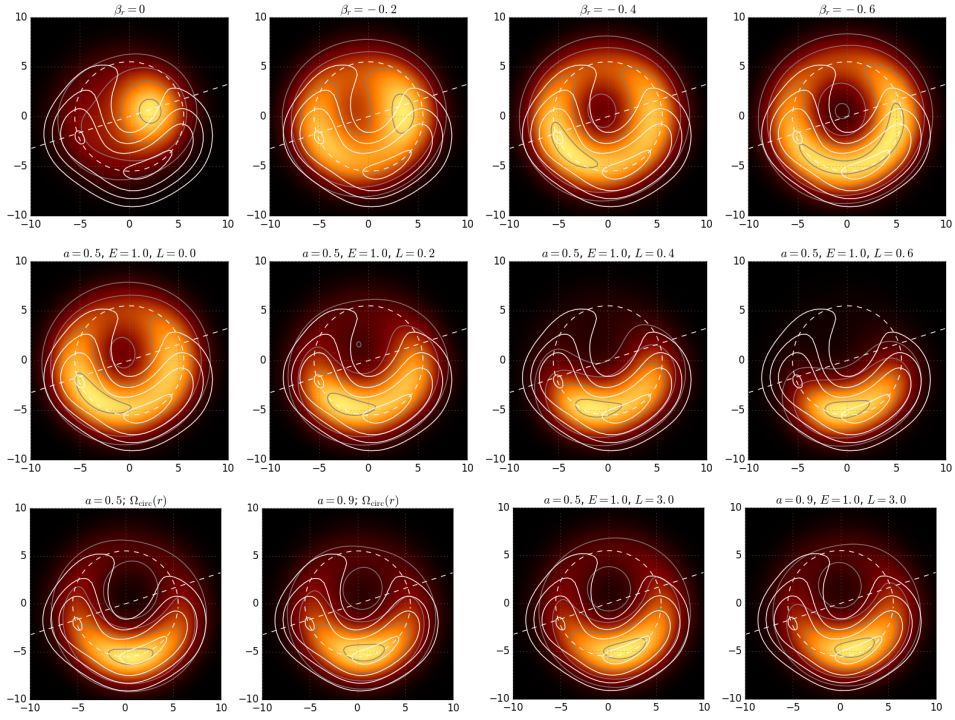

Fig. 1: Images of M87* calculated with our toy model (colour shading and grey contours) compared with the 2017 April 11th EHT observation of M87* (solid white contours). *Top row:* the case of polar caps (TH1) for $a = 0.5$, showing the effect of Doppler beaming due to radial infall of the emitting fluid with fixed radial velocity β_r. *Middle row:* the case of polar caps (TH1) for $a = 0.5$ with fixed values of conserved energy E and angular momentum L. *Bottom row:* the case of equatorial ring (TH4) for two values of BH spin, with different assumptions on the kinematics of the emitting fluid; *two left panels:* stable circular orbits with $\beta_r = 0$ and Keplerian angular velocity $\Omega_{\rm circ}(r)$ within prograde discs limited by $r_{\rm ISCO}(a) < r < r_{\rm max} = 6M$; *two right panels:* plunging orbits with conserved energy E and angular momentum L, limited by $r_{\rm h} < r < r_{\rm max} = 6M$. For all presented images, the contour levels correspond to brightness temperature values of $(2.5, 3.5, 4.5, 5.5)\times 10^9$ K. The dashed white circle indicates a photon ring of radius 21 μas $\simeq 5.5\theta_{\rm g}$. The dashed white line indicates the position angle $\mathrm{PA_{jet}} = 288^\circ$ of the large-scale jet. Adapted from Nalewajko et al. (2020).

an outer radius of $r_{\rm max} = 6R_{\rm g}$. Here, we consider two particular cases: *equatorial ring* with $\theta_{\rm min} = 75^\circ$ and $\theta_{\rm max} = 90^\circ$; and *polar caps* with $\theta_{\rm min} = 0$ and $\theta_{\rm max} = 30^\circ$. More details can be found in our article Nalewajko et al. (2020).

Results. The top row of panels in Fig. 1 presents the case of polar caps for the BH spin value of $a = 0.5$ and radial infall with different values of fixed coordinate velocity β_r. The image of the front cap is strongly suppressed for the radial velocity of $\beta_r \geq 0.4$, and we see the image of the back cap magnified into a ring that is slightly brighter on the southern side. This illustrates the basic fact that kinematics of emitting fluid, which involves mildly relativistic motions, has a very strong effect

on the appearance of BH environments.

The middle row of panels in Fig. 1 presents the case of polar caps for the BH spin value of $a = 0.5$ and fixed asymptotic energy $E = 1$, showing the effect of moderate angular momentum $0 < L < 0.6$. In the case of $E = 1$ and $L = 0$, we obtain a fairly uniform ring with maximum brightness in the SE sector. Introducing non-zero L has a very strong effect for decreasing the brightness along the northern side of the ring, turning it into a crescent already for $L = 0.2$. Higher values of L make the image too compact, centred in the S sector. Emission from the SEE sector is again very week for $L > 0$.

The bottom row of panels in Fig. 1 presents the case of equatorial ring, comparing two models of kinematics: (1) quasi-Keplerian circular motions with $\beta_r = 0$ and angular velocity $\Omega = \Omega_{\rm circ}$, with the rings limited from the inside by the innermost stable circular orbit (ISCO), or (2) plunging geodesic timelike flows with conserved energy E and angular momentum L; and for two values of BH spin $a = 0.5, 0.9$. It is notable that these images are very similar, with most emission concentrated along the southern side of the photon ring. Our models for plunging flows with fixed E and L provide very natural match with the observed emission in the SSE-SWW sector. Emission from the SEE sector is very weak in all simulated cases. It should be stressed that these results are not sensitive to the choice of E and L values, very similar images were obtained for $0.94 \leq E \leq 1.3$ and for $2 \leq L \leq 3.9$.

Conclusion. The origin of emission observed by the EHT in the SEE sector of the photon ring in M87* cannot be explained using strictly stationary and axisymmetric models – whether equatorial rings or polar caps – that assume the theoretically expected alignment of the BH spin with the large-scale jet, well constrained from observations.

Acknowledgements. We acknowledge discussions with Bartosz Bełdycki, Benoît Cerutti, Christian Fromm, Jean-Pierre Lasota and Maciej Wielgus. This work was partially supported by the Polish National Science Centre grants 2015/18/E/ST9/00580 and 2015/17/-B/ST9/03422.

References

EHT Collaboration, et al., *ApJ* **875**, 1, L1 (2019a)

EHT Collaboration, et al., *ApJ* **875**, 1, L5 (2019b)

Nalewajko, K., Sikora, M., Różańska, A., *A&A* **634**, A38 (2020)

Walker, R. C., et al., *ApJ* **855**, 2, 128 (2018)